1996A&A...305..970B

Astron. Astrophys. 305, 970–976 (1996)

ASTRONOMY AND ASTROPHYSICS

Very long baseline interferometry of solar microwave radiation

A.O. Benz[1], D. Graham[2], H. Isliker[1], C. Andersson[3], W. Köhnlein[4], F. Mantovani[5], and G. Umana[5]

[1] Institute of Astronomy, ETH, CH-8092 Zürich, Switzerland
[2] Max-Planck-Intitut für Radioastronomie, Auf dem Hügel 69, D-53121, Germany
[3] Onsala Space Observatory, S-43992 Onsala, Sweden
[4] Deutsche Forschungsanstalt für Luft- und Raumfahrt, Rudower Chaussee 5, NE-PE, D-12489 Berlin, Germany
[5] Istituto di Radioastronomia, P. Gobeti 101, I-40129 Bologna, Italy

Abstract. The solar 2.297 GHz radiation has been observed and investigated by very long baseline interferometry (VLBI). The radio observatories of Medicina, Noto, Onsala, and Weilheim were involved yielding baselines between 360 km and 3800 km and a nominal resolution of 0.09″to 0.008″or 70 to 6 km on the Sun. This solar VLBI network operated successfully with at least one useful baseline for 167 hours during five campaigns at the maximum of the most recent activity cycle in 1989 and 1990. The Phoenix spectrometer at Zurich was used to detect and classify the radio bursts. A total of 59 solar radio bursts were observed at the VLBI frequency, of which 26 events were analyzed, including narrowband millisecond spikes, type III bursts, patches, pulsations, and diffuse broadband (gyrosynchrotron) emission. Neither during bursts nor in quiet times significant fringes were detected. All sources were well resolved including the narrowband spikes. We interpret the result in terms of relatively large radio sources and/or by scattering to apparent source sizes larger than the lowest resolution and by the lack of 'speckles'. The results are consistent with scattering of the radio emission in the corona. The upper and lower limits of the source size of spikes are discussed. For the apparent source size, ℓ_a, we find 65 km $< \ell_a <$ 16 000 km, and for the original source size before scattering $\ell \lesssim$ 200 km.

Key words: Sun: radio radiation – Sun: flares – techniques: interferometric – scattering

1. Introduction

Some of the important physics of solar plasma processes, such as flare energy release, coronal heating and photospheric flows, take place on extremely small scales. Fine structure in X-ray images at 63.5Å (Fe XVI and Mg X) has been observed in the corona at all locations and down to the instrumental resolution of 0.75″ or 550 km (Golub et al. 1990). Small-scale magnetic patterns have been inferred to exist in the solar photosphere at a scale of less than 100 km (e.g. Stenflo 1994). Radio scintillation observations in the solar wind between $r \approx 2 - 22 R_\odot$ show structures below 1 km and considerable inhomogeneity in the 3–30 km range (e.g. Coles & Harmon 1989). Furthermore, small-scale processes have been suggested to cause narrowband coherent radio bursts in solar flares at extremely high brightness temperatures.

Coherent emission processes include plasma emission and gyromagnetic emission at the plasma frequency and the electron gyrofrequency, respectively, or their harmonics. These emission processes are intrinsically narrowband, so the observed bandwidth $\Delta\nu$ requires a source size smaller than $\Delta\nu/\nu$ times the length scale of variation of the relevant emission frequency in the source region. For narrowband microwave spikes this upper limit of the source size is $3 \cdot 10^{-3}$ of the length scale (Csillaghy & Benz 1993), or less than about 100 km. The total duration of the spikes, a few tens of milliseconds at 3 GHz, is consistent with the small source size, but its upper limit is higher.

Interferometric radio images of the Sun suffer from the following problems:

- The complexity of the image requires a good coverage of the u-v plane (Fourier space).
- The variability of the sources inhibits long integrations.
- Strong confusion sources in the primary beam add noise in quiet regions.
- Near-field effects.

For radio images of the non-flaring Sun, these effects limit the spatial resolution to several arcseconds. The best resolution has been achieved with observations during a solar eclipse when the above problems are greatly reduced. Such an image of the quiet and slowly varying Sun with 2.6″ resolution at 5 GHz shows no unresolved structure (Gary & Hurford 1987).

Bursts of solar radio emission may be observed by interferometers in a snapshot mode. As strong events well surpass the total quiet flux density of the Sun, confusion by other sources is negligible. The main problem is to catch an interesting event during the allocated telescope time. Whereas synchrotron events are frequent in the microwave region, coherent microwave events and, in particular, narrowband millisecond spikes are extremely

Send offprint requests to: A.O. Benz

© European Southern Observatory • Provided by the NASA Astrophysics Data System

1996A&A...305..970B

rare even in years of maximum solar activity. Narrowband spikes have been observed with the one-dimensional Westerbork interferometer at 608 MHz by Kaastra (1985). The sources were found to be smaller than the instrumental resolution of 14″ (or 10^9 cm). Gary et al. (1991) observed unclassified bursts (possibly including narrowband spikes) at 2.8 GHz, measuring less than the instrumental resolution of 28″ in one dimension. Narrowband spikes in the decimetric and microwave bands have never been spatially resolved. They are of particular interest due to their correlation with hard X-ray emission and their possible close association with flare energy release (review by Benz 1986).

Other burst types, however, have been resolved. Krucker et al. (1995) measured with the VLA at 333 MHz a *metric* spike size of 68″. Type III observations at 1.4 GHz with the VLA show resolved source sizes of some tens of arcseconds at FWHP (e.g. Aschwanden et al. 1992, 1993). Highly polarized decimetric pulsations have been resolved having a FWHP of 8″ (Willson et al. 1992). Sources of incoherent gyrosynchrotron radiation are well known to have source sizes of 3 – 20″ at 4.9 GHz and larger than 30″ at 1.4 GHz (review by Alissandrakis 1986).

The propagation of radio waves through an inhomogeneous corona may considerably increase both the apparent source area, A, and the solid angle, $\Delta\Omega$, to which the radiation is confined (e.g. Bastian 1994 and references therein). However, little is known about inhomogeneity in the low corona, and no systematic studies of scattering exist below 2 solar radii. Furthermore, Liouville's theorem requires that the product $A\ \Delta\Omega$ remains constant (Melrose & Dulk 1988). The inconsistency disappears if the apparent source has a small filling factor, in other words, if the instantaneous images consist of 'speckles'. Such structures may be observable by VLBI in short duration bursts, as for example in narrowband spikes.

Very Long Baseline Interferometry (VLBI) observations of solar radio bursts at 18 cm have been reported by Tapping et al. (1983) and Tapping (1986). A single, 1630 km baseline was used and a total of three small peaks (of order 10 sfu = 10^5 Jy = 10^{-18} erg/s cm^2 Hz) were registered. In none of these unclassified bursts significant interferometric fringes were detected. However, the authors have noted that during the event the peak amplitude of the correlator output seems to occur within a reduced set of delay channels. Although this was not a real detection of sub-arcsecond structure, it warrants further investigations and has motivated this experiment.

Here we present new VLBI observations of solar radio bursts recorded by a multiple baseline network at 13 cm during the peak of the most recent activity cycle. The network observed many weak and strong events, which we were able to classify using a spectrometer. The discussion finally concentrates on observations of narrowband spikes.

2. Observation

VLBI is a powerful technique to achieve sub-arcsecond resolution by a set of single, not physically connected antennas. Contrary to galactic and extragalactic VLBI, observations of the relatively strong solar radio bursts do not require large antennas. The data and atomic timing are recorded on magnetic tape at each antenna and cross-correlated at a central processor.

2.1. The solar VLBI network

A network of four VLBI antennas was set up for solar observations at 2.297 GHz (13 cm). It included: Noto (Sicily, Southern Italy) 32 m dish; Medicina (Northern Italy) 32 m; Onsala (Sweden) 25 m; Weilheim (Germany) 30 m. The antennas were pointed to the center of the Sun. Even for the biggest dishes, the Sun was within twice the FWHP of the antenna beam. As the Sun contributed the dominant component of the receivers' input, the receiver gains were reduced by omitting the front-end amplifiers and/or adding attenuation at the intermediate frequency stage.

The observations were carried out during five weeks spread between 1989 September 19 and 1990 October 10. Each campaign lasted typically five days of dawn to dusk observations, each preceded and followed by a calibration on 3C84, 3C273, or 3C345. The set of antennas was not always complete, as some joined later, were unavailable, or had technical problems. This solar VLBI network operated successfully with at least one useful baseline for a total of 167 hours.

The Mark II VLBI system was used, yielding a bandwidth of 2 MHz. A readable summary of its operation has been given by Alef (1989). The recorded sense of polarization was right hand circular.

2.2. Spectrometer

The radio spectrometer Phoenix of ETH Zurich (Benz et al. 1991) was programmed to observe the frequency range from 2.17 to 2.42 GHz during the VLBI campaigns. The spectrometer was operated in Dicke mode, switching to a thermal load at a rate of 10 kHz. The spectrum was recorded in 25 channels of 10 MHz bandwidth. Each channel was sampled every 12.5 ms; and eight samples were integrated on-line to yield an effective time resolution of 0.1 s. The total flux density, left plus right hand circular polarization, was recorded. Flux and polarization were calibrated in two steps involving an internal noise source and the slowly varying Sun.

The spectrograms of the solar background radiation have an rms noise of 1.8 sfu. They were used to search for radio bursts and to classify them according to the survey by Isliker and Benz (1994). This information was essential for the selection of VLBI time intervals to be correlated and further studied.

2.3. Correlation

As the background of the solar disk is well-known to have no sub-arcsecond structures, its contribution cancels when the signals received at two telescopes are cross-correlated. The small sources sought in this experiment are comparable in flux density to the background of the whole solar disk and exceed it in

© European Southern Observatory • Provided by the NASA Astrophysics Data System

1996A&A...305..970B

brightness temperature by many orders of magnitude. As these bursting sources are transient, the highest time resolution available, 0.2 s, was used for correlation.

Assuming that the source is in the far field of a two-antenna baseline, the arrival of the signal at the second antenna of a pair is delayed in relation to the first antenna by

$$\tau = \frac{b}{c}(\sin\delta_b \ \sin\delta_s + cos\delta_b \ \cos\delta_s \ \cos h) \ , \qquad (1)$$

where b is the baseline (distance between the two antennas) and c is the speed of light. The declination of the second antenna as viewed from the first is δ_b, the declination of the source δ_s, and $h = H_s - H_b$, where H_b is the hour angle of the second antenna as viewed from the first, and H_s is the hour angle of the source.

The near-field correction to the delay of the signal at the second antenna, $\Delta\tau$, due to the curvature of the wave fronts is

$$\Delta\tau = \frac{(b\cos\alpha)^2}{2\,c\,D} \ , \qquad (2)$$

where D is the distance to the source and $b\cos\alpha$ is the projected baseline on the plane perpendicular to the line through the first antenna and the source. The far-field condition, $\Delta\tau c/\lambda < 0.1$, is not satisfied for all of our baselines. However, the correction (Eq. 2) is a few nanoseconds and its main effect is to shift the source by at most 2.6″ from the apparent position in the far-field approximation. Since we do not map the source using different baselines, the near-field effect can be neglected.

The cross-correlation between the signals of two antennas is a function of the delay. Since the Earth rotates and moves around the Sun, the angles δ_b and h in Eq. (1) and therefore the delay changes with time. When the signals of the two antennas are cross-correlated for a fixed position on the sky, the output is a quasi-periodic function in time called 'fringes'. The solar rotation is a minor effect and, together with unknown peculiar source motions, has been neglected.

The fringe rate at which the source moves through the fringe pattern is given by the position on the solar disk, estimated from the position of the associated $H\alpha$ flare (Solar and Geophysical Data 1990). The difference between the actual and estimated positions leads to differences between the actual and predicted delays and fringe rates. The positional uncertainty is treated by using up to 128 different delay windows and fringe rates, called 'delay channels'. These channels correspond to different one-dimensional positions covering a range of ±3.1′ to ±36.7′ centered at the most probable location. The range depends on the projected baseline length and the correlator setup. In cases of several possible flare sites, fringes were searched for the different locations.

The data were correlated at the Mk II correlator in Bonn. The amplitude of the raw, complex correlated signal in each channel was calculated. Its amplitude, after calibration, is the correlated flux density, possibly reduced from the total flux by spatial extension of the source. It may be compared to the total flux density observed by the spectrometer to estimate the source size. The output of the correlator is a fringe amplitude per time interval, 0.2 s, and per delay channel (i.e. position). This two-dimensional array is searched for enhanced values, i.e. significant correlated flux during intervals of solar radio bursts.

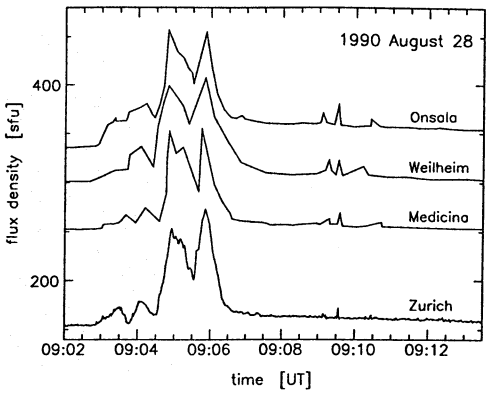

Fig. 1. Flux density vs. time of solar flare radio emission at 2.3 GHz. The top three curves show the outputs of some single VLBI antennas scaled by a factor of two since they observe only right hand circular polarization. The bottom curve presents the calibrated observation in the 2.295 GHz left + right hand circular polarization channel of the Zurich spectrometer (Phoenix)

3. Data analysis and results

3.1. Data selection

During the 167 hours of VLBI observing the Phoenix spectrometer has registered 59 groups of solar radio events consisting of hundreds of single bursts. Using the scheme of Isliker & Benz (1994) we classified them into 2 events of narrowband spikes, 28 groups of type III bursts, 2 pulsations, 12 groups of patches, and 16 events of synchrotron emission. The most interesting events of each class have been selected for correlation (cf. Table I).

An example of the total power recordings by single VLBI antennas is presented in Fig. 1. The plots, digitized chart recorder outputs, have been compared with the calibrated 2.295 GHz channel of the Zurich spectrometer, integrated to 50 MHz bandwidth and 1s time resolution. The VLBI antennas measure only right hand circular polarization, the spectrometer recorded only the sum of left and right circular polarization. It has been used to calibrate the flux of the outputs of the VLBI antennas and to estimate the polarization of the emission. The prominent peaks at 09:05 UT are broadband in the spectrum, and thus appear to be synchrotron emission. Therefore they have presumably low polarization (e.g. review by Alissandrakis 1986). The small peaks between 09:09 and 09:11 UT (shown in detail in Fig.2) are relatively large in the single VLBI antenna recordings compared to the spectrometer flux, indicating that they are strongly, right hand circularly polarized.

Figure 2 (top) shows an interesting part of the spectrogram of the event of Fig. 1. The single bursts have half-power bandwidths of 36–88 MHz, with an average of 63 MHz, thus 2.8 ± 0.8% of 2.3 GHz, the observing frequency. This agrees

© European Southern Observatory • Provided by the NASA Astrophysics Data System

1996A&A...305..970B

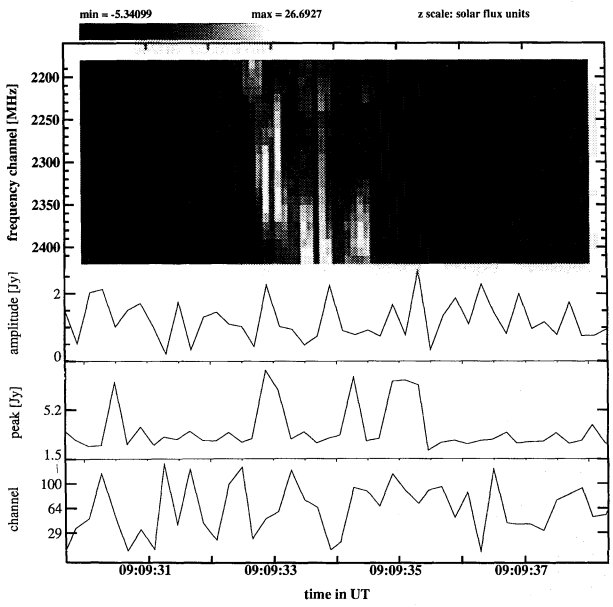

Fig. 2. Solar VLBI observations compared to spectrogram. **Top**: The total power registration of the Zurich spectrometer of a part of the 1990 August 28 event (Fig. 1) is presented in frequency vs. time. Enhanced solar emission appears bright with the scale (in sfu) given at the top. The solar bursts are classified as a group of about a dozen narrowband spikes. **Second**: Fringe amplitude of the Weilheim-Medicina baseline in jansky (10^{-4} sfu) at the most likely source position. **Third**: Peak fringe amplitude in each 0.2 second time step over the whole solar disk. **Bottom**: Channel number of peak amplitude

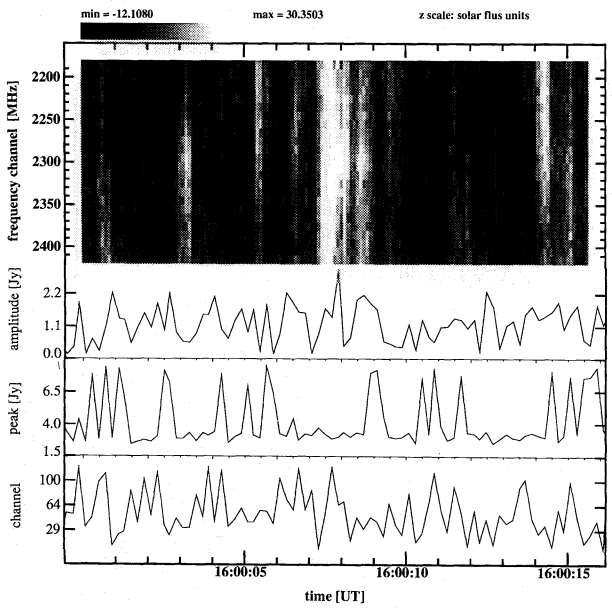

Fig. 3. Similar to Fig. 2 showing a group of solar microwave type III bursts that occurred on 1990 August 27

with the results of Csillaghy & Benz (1993) for narrowband spikes. The bursts have not been resolved in time at a resolution of 100 ms, compatible with the average duration

$$d(\nu) \approx 0.049\left(\frac{\nu}{661\ \mathrm{MHz}}\right)^{-1.34\pm0.13} \quad [\mathrm{s}] \qquad (3)$$

derived by Güdel & Benz (1990) for spikes in the 0.3–1 GHz range. At 2.3 GHz Eq. (3) predicts a duration of 8–11 ms. The flux observed by the spectrometer is an average over 100 ms and thus considerably smaller than the peak. Polarization (Fig. 1), bandwidth, and duration strongly suggest that the emission must be classified as narrowband microwave spikes.

A different example is presented in Fig. 3. The bandwidth of some bursts exceeds the observed range of the spectrometer of 250 MHz. The maximum seems to drift with time and frequency, but the drift rate is of the order of the instrumental resolution, 2 GHz/s. Both signs of drift, corresponding to upward and downward motions in the corona, are discernible. These characteristics suggest that the event presented in Fig. 3 must be classified as a group of microwave type III bursts.

3.2. Correlated flux density

The correlated flux density (fringe amplitude) of the spike event in the complex delay channel corresponding to the most likely position ($\pm 2'$) is shown in the second panel of Fig. 2. No enhancement of correlated flux density during the bursts is seen. The background level and the fluctuations are entirely consistent with the Rayleigh distributed noise expected from one-bit correlation in the case of a completely resolved source. The upper limit (7σ) of correlated burst emission is $4.2 \cdot 10^{-4}$ sfu.

The third panel of Fig. 2 displays the largest peak amplitude in each 0.2 second time interval found in any of the 128 delay channels, covering a strip of $73.'4$ and including the whole solar disk. The time profile does not show a significant peak during the radio bursts with an upper limit of $9 \cdot 10^{-4}$ sfu. The non-statistical appearance of this plot appears to be an artefact associated with occasional parity errors in the replayed data.

Finally, the bottom panel of Fig. 2 displays the delay channel number with peak fringe amplitude in the 0.2 s time step. If a marginal contribution of correlated flux density existed, one would expect the channel numbers to converge to a particular value. This idea has been used by Tapping et al. (1983). Figure 2 does not show such an effect although this event was stronger than their bursts and richer in spikes.

Figure 3 and the other selected events have been investigated in the same way with similar results listed in Table 1. In no event was significant correlated flux detected. A lower limit of the source size is evaluated from this null result in the following section.

3.3. Lower limit of size

Let us assume that the source intensity has a Gaussian shape with an angular width δ (source size),

$$I(\phi) = \frac{F}{\sqrt{\pi}\,\delta}\ \exp\left[-\left(\frac{\phi}{\delta}\right)^2\right], \qquad (4)$$

© European Southern Observatory • Provided by the NASA Astrophysics Data System

1996A&A...305..970B

Table 1. Selected events for VLBI analysis and results. The peak flux density at 2.295 GHz is given for the indicated burst type. The upper limit of the correlated flux in the smallest available baseline is given by 7σ of the fringe amplitude measured during the interval of interest in the most likely position channel with a time resolution of 0.2 seconds. (GG = large group, RS = reversed drift, U = type U burst)

date	time [UT]	duration [s]	burst type	flux density [sfu]	upper limit of correlated flux [10^{-4}sfu = 1 Jy]
89/09/19	08:14:28–08:15:10		g.synchrotron	14	3.9
	09:54:20–09:57:40		g.synchrotron	37	4.3
	10:36:00–10:47:30		g.synchrotron	50	4.2
	10:40:10–10:41:40		type III, U	32	4.2
	11:22:11–11:24:40		type III	9	4.5
	12:31:36–12:32:00		type III, GG	13	4.7
	16:08:47–16:08:49		type III		5.0
	16:10:18–16:10:33		type III		5.0
	16:13:55–16:14:10		type III		5.0
	16:18:38–16:18:40		type III		5.0
90/08/27	10:33:19–10:34:33		patch	15	4.4
	15:59:15–16:01:23		g.synchrotron	124	4.5
	15:59:24–16:00:22		type III	35	4.7
90/08/28	09:02:00–10:00:00		g.synchrotron	140	4.8
	09:03:03–09:06:18		type III	13	4.8
	09:09:01–09:09:09		type III	16	3.9
	09:09:32–09:10:39		spikes	27	4.2
	09:12:22–09:19:15		patch	32	4.2
	10:10:57–10:16:42		g.synchrotron	75	4.5
	10:13:26–10:18:16		type III, GG	18	4.4
	12:47:36–12:51:13		g.synchrotron	79	4.1
	14:27:07–14:30:53		g.synchrotron	34	4.6
	14:28:13–14:28:31		type III, RS	21	4.4
	16:18:07–16:19:05		type III	17	4.2

where F is the total flux density observed e.g. by the spectrometer. The visibility $\mathscr{V}$ is defined as the ratio of the correlated flux to the total flux. It is given by the convolution of the source with the fringe pattern at zero lag,

$$\mathscr{V} = \frac{1}{\sqrt{\pi}\,\delta} \int_{-\pi}^{+\pi} \exp[-\left(\frac{\phi}{\delta}\right)^2] \cos(2\pi\frac{\phi}{\phi_0})\mathrm{d}\phi \ . \qquad (5)$$

ϕ_0 is the fringe spacing, $\lambda/(b\,\cos\alpha)$; and $\phi_0 \ll 1$ rad has been assumed. The visibility becomes exceedingly small if the source size exceeds the fringe spacing (Fig. 4).

We have simulated the effect of speckles on the visibility of sources with $\delta \gg \phi_0$. As a rough approximation the (one dimensional) source was modulated by a function $(1 + \cos[2\pi\phi/\eta])$, where η is the size of the speckles. The resulting deviation in visibility is small and marginally noticeable in Fig. 4 around a source size of 10 mas. The only exception was found for $\eta = n\phi_0$, $n = 1, 2, \ldots$, where it reached e.g. $\mathscr{V} = 0.003$ for $n = 1$, $\phi_0 = 89$ mas, and $\delta = 3'$. This beating between speckle pattern and fringe pattern is, however, unrealistic and can be neglected. Figure 4 suggests that speckles, if distributed randomly over a large source, cannot be detected by this VLBI setup.

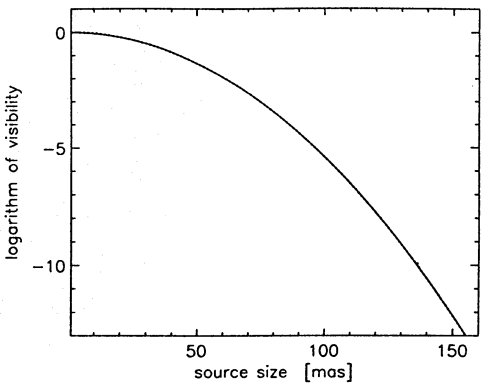

Fig. 4. The visibility of a Gaussian model source is presented vs. source size in milliarcseconds (mas). A fringe spacing of 89 mas has been assumed, corresponding to our smallest baselength and the observing frequency. The dotted curve shows a Gaussian model modulated by a sinusoid with a wavelength of 20 mas to simulate speckles

Since $\mathscr{V} < 7\sigma/F$, where σ is the rms noise of the background fringe amplitude, Eq. (5) can be solved to yield a lower limit of the $1/e$-source size δ. The results listed in Table 1 yield typically $\mathscr{V} \lesssim 3 \cdot 10^{-5}$, thus $\delta \gtrsim 90$ mas (Fig. 4).

© European Southern Observatory • Provided by the NASA Astrophysics Data System

1996A&A...305..970B

3.4. Sub-megahertz spectral resolution

As a by-product the data of single VLBI stations also contain spectral information. The spectrum in the 2 MHz observing band has been extracted by Fourier transforming the autocorrelation function. A spectral resolution of 20 kHz has been achieved. To our knowledge, this is by far the highest resolution at which the solar microwave radiation has ever been observed. The standard deviation in the 2 MHz wide spectrograms was 1.5% of the background or about 3 sfu. However, no spectral feature smaller than 2 MHz has been detected. Thus our measurements show the absence of spectral fine structures above 9 sfu even during the group of narrowband spikes on 1990/08/28 (Figs. 1 and 2).

4. Discussion and conclusions

4.1. Lower and upper limits of source size

Our VLBI experiment has not detected any spatial structure in the solar radio emission smaller than 0.09″ (or 65 km on the Sun). The upper limit of the correlated flux was a few 10^{-4} sfu (janskys) for the quiet Sun and various bursts at a frequency of 2.297 GHz. The size of 65 km is therefore a lower limit to the apparent radio sources and spatial structures of the solar radio emission at this frequency.

In the following we will concentrate on the group of narrowband spikes observed on 1990 August 28 (Figs. 1 and 2). The narrow bandwidth suggests an upper limit of the source size by the assumption that the emission is at a characteristic frequency of the plasma (most likely the electron gyrofrequency or a harmonic). The bandwidth is then caused by the variation of that frequency throughout the source plus the unknown natural bandwidth of the emission process. Thus, the original source size before scattering

$$\ell < \frac{\Delta\nu}{\nu} H = 160 - 380 \left(\frac{H}{10^9 \text{ cm}} \right) \text{ [km]} \ , \qquad (6)$$

where H is the scale length of the characteristic frequency. In Eq.(6) we have used the observed FWHP of the spikes, spanning a range of 36–88 MHz in the observed event. For gyroemission H is the scale length of the magnetic field. Note that Eq.(6) gives a limit on the original source size and that H may be an order of magnitude smaller than 10^9 cm, but probably not much larger.

4.2. Scattering by plasma inhomogeneities

Do these upper and lower limits suggest that spike sources have a diameter of about 100 km? VLA observations of metric spikes, which occur at much lower frequency and are possibly caused by a different physical process, have seen much bigger sources (Krucker et al. 1995). Therefore, we discuss the possibility that the apparent source sizes measured by radio interferometry are enhanced by scattering in the corona. Small fluctuations in density and/or magnetic field distort a propagating wave as the wave phases of adjacent rays propagate at different speeds. The wave fronts break up into parts that are deflected, focussed and defocused in a random way.

The theory of wave propagation in a continuous, random medium has been treated in a number of books, most recently by Rytov et al. (1989), and its application to astrophysics has been reviewed e.g. by Rickett (1990). Bastian (1994) has recently adapted it to solar radio emission and used it to interpret the reduced contrast of solar radio images compared to soft X-rays.

The density fluctuations of the outer solar corona have been determined from the scintillations of background sources. The distribution is a power-law of the Kolmogorov type at scales larger than a few hundred kilometers, becomes flatter at smaller scales and decreases at an 'inner scale' of about 1 km at $r \approx 3R_\odot$ (Coles & Harmon 1989). Bastian has calculated the broadening of the image of a point source in the corona by multiple, small-angle scatterings extrapolating from the observed density fluctuations and neglecting magnetic effects. He finds for the FWHP apparent size of a point source at 2.297 GHz and in the disk center (consistent with the 90/08/28 flare at N15 E15) $\delta_a = 4''$ to $20''$, given by the possible range of parameters.

The apparent source size δ_a can be derived independently from the decay time τ_s of a sharply peaked signal due to the multi-path effect of scattering. A geometric argument (Ratcliffe 1956; for a simple derivation cf. Benz 1993) gives the relation

$$\tau_s \approx \frac{D^2}{D_1} \frac{\delta_a^2}{2c} \ , \qquad (7)$$

where δ_a is in units of radians. The distance D from the source to the observer has been assumed to be much larger than the distance D_1 from the source to the scattering medium.

As the size δ_a of a scattered image decreases with ν^{-2} (e.g. Benz 1993), Eq. (7) predicts a frequency dependence of $\tau_s \propto \nu^{-4}$. However, observations in the 0.3–1.0 GHz range (Güdel & Benz 1990) and unpublished data at 1–2 GHz show that the spike decay time follows the law $\tau_0 \approx 10.6\, \nu^{-1.06}$ [ms]. Thus, the observed decay time seems to be intrinsic to the source and not caused by scattering. Therefore, we require $\tau_s \ll \tau_0$.

Equation (7) then gives an apparent source size of

$$\ell_a = D\delta_a < \sqrt{2cD_1\tau_0} \ . \qquad (8)$$

Using the coronal density scale height $H_n \approx 10^{10}$ cm as an approximation for D_1 and $\tau_0 \approx 4$ ms at 2.297 GHz, we find $\ell_a < 16\,000$ km (or $< 22''$) in agreement with the values derived theoretically by Bastian (1994).

4.3. Brightness temperature of spike sources

The brightness temperature, T_b, of spike sources has been calculated from theory using various saturation processes of the electron cyclotron maser theory. Melrose & Dulk (1982) and others have derived $T_b \lesssim 10^{17}$ K. This has been confirmed by numerical simulations of quasi-linear diffusion most recently

© European Southern Observatory • Provided by the NASA Astrophysics Data System

1996A&A...305..970B

by Aschwanden (1990) who finds T_b up to $3 \cdot 10^{18}$ K and typical source sizes of 100 km.

The brightness temperature of a fully polarized solar source with a flux density S is

$$T_b = \frac{2c^2}{\pi\, k_B\, \nu^2} \left(\frac{D}{\ell}\right)^2 S = 9.28 \cdot 10^{15} \nu_{\rm GHz}^{-2} S_{\rm sfu} \ell_{\rm km}^{-2}\ [\rm K]\,, \qquad (9)$$

in the Rayleigh-Jeans approximation. Using the observed values for the spikes on 90/08/28, the upper limit on the original source dimension, and $H = 10^9$ cm (Eq.6), the highest brightness temperature in the source exceeds $T_b > 1.9 \cdot 10^{12}$ K, consistent with theory.

The VLBI measurements yield an upper limit of the *apparent* brightness temperature (after propagation, scattering and absorption) of $T_{ba} < 1.1 \cdot 10^{13}$ K.

4.4. Observations of speckles

If the radio images at 2.297 GHz are broadened by scattering, why did the VLBI observations not reveal any speckles? There are at least two reasons:

1. The numerical simulations in Sect. 3.3 have shown that one baseline cannot resolve a pattern of small speckles unless it occurs at a regular period.
2. The pattern of speckles changes with frequency. The spatial variations due to scattering are therefore not the same if observed at two frequencies separated by more than the decorrelation bandwidth,

$$\Delta\nu \approx \frac{1}{2\pi\, \tau_s}\,. \qquad (10)$$

The scattering decay time τ_s can be estimated by Eq.(7). Using $\delta_a \approx 10''$ at 2.297 GHz and $D_1 \approx H_n \approx 10^{10}$ cm, $\tau_s \approx 1$ ms, Eq.(10) yields $\Delta\nu \approx 160$ Hz. Since the observing bandwidth of the VLBI experiment was 2 MHz, the speckles (if any) have been smeared out.

This VLBI experiment did not record any spatial coherence of the spike source, e.g. produced by a regular pattern of speckles.

In conclusion, these observations are consistent with solar radio spike sources smaller than a few hundred kilometers (or $\lesssim 0.3''$) and apparent (scattered) source sizes between $0.09''$ and about $10''$at 2.3 GHz. Future spike observations (not necessarily VLBI) at arcsecond resolution may yield quantitative constraints on the plasma inhomogeneity of the innermost corona.

Acknowledgements. J. Brunner helped with the spectrometer observations. We also thank M.J. Aschwanden for helpful comments on an early version of the manuscript, and G. Belvedere and the Catania solar observatory group for providing $H\alpha$ flare positions. The construction and development of the ETH Zürich spectrometers and the work of H.I. are financially supported by the Swiss National Science Foundation Grant Nr. 20-040336.94.

References

Alef W., 1989, in: Very Long Baseline Interferometry, eds. M. Felli and R.E. Spencer, Kluwer Acad.Publ., Dordrecht, p.45
Alissandrakis C.E., 1986, Solar Phys. 104, 207
Aschwanden M.J., 1990, A&A 237, 512
Aschwanden M.J., Bastian T.S., Benz A.O., Brosius J.W., 1992, ApJ 391, 380
Aschwanden M.J., Benz A.O., Schwarz R.A., 1993, ApJ 417, 790
Bastian T.S., 1989, in: Synthesis Imaging in Radio Astronomy, eds. R.A. Perley et al., ASP Conf.Ser. Vol. 6, p. 395
Bastian T.S., 1994, ApJ 426, 774
Benz A.O., 1986, Solar Phys. 104, 99
Benz A.O., 1993, Plasma Astrophysics, Kluwer Acad.Publ., Dordrecht, chapt. 11.4
Benz A.O., Güdel M., Isliker H., Miszkowicz S., Stehling W., 1991, Solar Phys. 133, 385
Coles W.A., Harmon J.K., 1989, ApJ 337, 1023
Csillaghy A., Benz A.O., 1993, A&A 274, 487
Gary D.E., Hurford G.J., 1987, ApJ 317, 522
Gary D.E., Hurford G.J., Flees D., 1991, ApJ 369, 255
Golub L. et al., 1990, Nature 344, 842
Isliker H., Benz A.O., 1994, A&AS 104, 145
Kaastra J.S., 1985, dissertation, Utrecht, p.151
Krucker S., Aschwanden M.J., Bastian T.S., Benz A.O., 1995, A&A, in press
Melrose D.B., Dulk G.A., 1988, Solar Phys. 116, 141
Melrose D.B., Dulk G.A., 1982, ApJ 259, 844
Ratcliffe J.A., 1956, Rept.Prog.Phys. 19, 188
Rickett B.J., 1990, ARA&A 28, 561
Rytov S.M., Kravtsov Yu. A., Tatarskii V.I., 1989, in: Principle of Statistical Radiophysics, Vol. 4, Springer-Verlag, Berlin
Solar and Geophysical Data, 1990, NOAA prompt reports 553, 43
Stenflo J.O., 1994, Solar Magnetic Field, Kluwer Acad.Publ., Dordrecht, chapt. 12
Tapping K.F., 1986, Solar Phys. 104, 199
Tapping K.F., Kuijpers J., Kaastra K.S. et al., 1983, A&A 122, 177
Willson, R.F., Aschwanden M.J., Benz A.O., 1992, NASA-CP 3137, 515

This article was processed by the author using Springer-Verlag TEX A&A macro package 1992.

© European Southern Observatory • Provided by the NASA Astrophysics Data System